bonding in **5a-5c** atom C(1) uses hybrids with a large p-content in these functions, and concomitantly orbitals with more s-character in the bonding to the terminal carbons. This may also explain the shorter bond distances between the central carbon and the radical terminals in **5a-5c** as compared to trimethylene.

Conclusions

On the basis of the results obtained by our calculations we arrive at the following conclusions:

(1) The thermal degenerate rearrangement in methylenecyclobutane is a two-step process going through a diradical intermediate of nearly C_s symmetry. The intermediate is stabilized by π-electron delocalization in the allylic moiety.

(2) The TS from methylenecyclobutane to the intermediate has C_1 symmetry with one of the two CH_2 groups in the allylic unit forming a π bond with the central carbon atom and the other being orthogonal to this CH_2-C plane. Its energy is found to be around 14 kcal/mol above the intermediate in the CASSCF calculation. This destabilization is mainly due to the breaking of the π-electron delocalization in the allylic unit.

(3) The singlet UHF wave functions for the intermediate and the TS were found to have extensive contaminations of the quintet state arising from coupling of the quartet component of the allylic fragment electrons with the lone electron on the migrating group.

(4) Exploratory UHF calculations on the conversion of spiropentane to methylenecyclobutane indicate that the reaction starts with a peripheral bond cleavage.

Acknowledgment. One of us (P.N.S.) thanks the Institute for Molecular Science for facilities placed at his disposal and for hospitality enjoyed during the period this work was carried out. He would also like to thank the Scandinavia-Japan Sasakawa Foundation for a generous grant that made it possible to carry through this project. We would like to thank Professor Yamaguchi for enlightening discussions on approximate spin projections. The numerical calculations were carried out at the Computer Center of IMS.

Appendix

In the extended Yamaguchi scheme the ^{1}UHF wave function is approximated by

$$^1\text{UHF} = a\,^1\text{PUHF} + b\,^3\text{PUHF} + c\,^5\text{UHF}$$

where a, b, and c are coefficients. Similarly the ^{3}UHF wave function is expressed as

$$^3\text{UHF} = d\,^3\text{PUHF} + e\,^5\text{UHF}$$

where d and e are coefficients. By using the conditions for the expectation values of the S^2 operator

$$\langle S^2(^1\text{UHF})\rangle = 2b^2 + 6c^2$$

$$\langle S^2(^1\text{UHF, triplet projection})\rangle = 6c^2/(a^2 + c^2)$$

$$\langle S^2(^3\text{UHF})\rangle = 2d^2 + 6e^2$$

and the normalization conditions of ^{1}UHF and ^{3}UHF, one can calculate the absolute values of the coefficients. Then, the energy of the approximately projected singlet is given by

$$E(^1\text{PUHF}) = \frac{1}{a^2}[E(^1\text{UHF}) - b^2E(^3\text{PUHF}) - c^2E(^5\text{UHF})]$$

By this procedure we obtained for **7** the spin-state weights (a^2, b^2, c^2) of (0.693, 0.181, 0.126) and (0.714, 0.148, 0.138) and a lowering of the ^{1}UHF energy amounting to 14.9 and 15.6 kcal/mol for the 3-21G and 6-31G basis sets, respectively.

The coefficients a-e are not very sensitive to the correlation correction. Therefore, the UHF values for the coefficients are used at UMP levels as well.

Registry No. **1**, 1120-56-5; **2**, 157-40-4.

Linear Semibridging Carbonyls. 2. Heterobimetallic Complexes Containing a Coordinatively Unsaturated Late Transition Metal Center

Andrew L. Sargent and Michael B. Hall*

Contribution from the Department of Chemistry, Texas A&M University, College Station, Texas 77843. *Received June 20, 1988*

Abstract: The electronic structure and bonding of four heterobimetallic carbonyl complexes, (tmed)$CuCo(CO)_4$, $(PPh_3)_2CuMo(CO)_3(\eta^5\text{-}C_5H_5)$, $(PPh_3)_2MoRh(CO)_3(\eta^5\text{-}C_5H_5)$, and (tmed)$CuMo(CO)_3(\eta^5\text{-}C_5H_5)$, are analyzed by the parameter-free Fenske-Hall molecular orbital method. The distinguishing characteristics of these four complexes are that one of the metal centers is a coordinatively unsaturated late transition metal center and that one or more carbonyls linearly semibridge the metal-metal bond. Coordinatively unsaturated late transition metal centers have been thought to accept electron density from semibridging carbonyl ligands to satisfy the 18-electron rule. Our results, however, suggest that these centers *donate* electron density from a high energy occupied metal dπ orbital to the unoccupied π^* orbitals of the linear semibridging carbonyl ligands.

Two basic types of bonding representations for unsymmetrically bridging homobimetallic carbonyl complexes have appeared in the literature and only recently does there seem to be some agreement on which representation is more accurate. The heart of the discrepancy concerns the direction of electron density flow between the metals and the bridging ligand, i.e., whether the bridging carbonyl donates electron density to or accepts electron density from the secondary metal center.

The first representation described the asymmetrically bridging carbonyl ligand in $Mn_2(CO)_5(dpm)_2$ (dpm = (diphenylphosphino)methane) as a four-electron donor, with two electrons donated from a CO σ orbital to one Mn atom and two electrons donated from a CO π orbital to the other Mn atom.[1] The donation of electrons from the CO π orbital was thought to be similar to metal-olefin bonding in complexes such as Zeise's salt and was necessary to achieve an 18-electron count around each metal atom.

The next representation to appear in the literature described the role of the unsymmetrically bridging carbonyl ligands as electron acceptors rather than electron donors.[2] The bonding

(1) Colton, R.; Commons, C. J. *Aust. J. Chem.* **1975**, *28*, 1673. Commons, C. J.; Hoskins, B. F. *Aust. J. Chem.* **1975**, *28*, 1663. Colton, R.; Commons, C. J.; Hoskins, B. F. *J. Chem. Soc., Chem. Commun.* **1975**, 363.

0002-7863/89/1511-1563$01.50/0

in several homobimetallic complexes was described, most notably the bonding in $(\eta^5\text{-}C_5H_5)_2V_2(CO)_5$. The basic model proposed that the asymmetrically bridging or "semibridging" CO groups accepted electron density in their π^* orbitals from the secondary metal center to mitigate the charge imbalance resulting from a dative metal–metal interaction.

The four-electron-donor model later reemerged to describe the bonding in various $(\eta^5\text{-}C_5H_5)_2M_2(CO)_4$ complexes,[3] including a reassessment of the bonding in the $(\eta^5\text{-}C_5H_5)_2V_2(CO)_5$ complex mentioned above.[3a]

The uncertainty regarding the nature of the carbonyl bonding in complexes with unsymmetrically bridging carbonyl ligands prompted several theoretical studies,[4-6] all of which concluded that the carbonyl π^* orbitals act as electron acceptors. The large energy gap between the metal d orbitals and the carbonyl π orbitals precludes any significant interaction between the two, whereas the close relative proximity of the CO π^* and metal d orbitals permit significant interaction. In addition, the interaction of the metal with the π^* orbitals is preferred over the interaction of the metal with the π orbitals based on overlap arguments since the π^* orbitals are predominantly carbon 2p in character while the π orbitals are predominantly oxygen 2p in character.

The extension of the bonding representation in which CO π^* orbitals are electron acceptors to heterobimetallic complexes with asymmetrically bridging carbonyls is not obvious, especially if the secondary metal center is coordinatively unsaturated and contains a late transition metal atom. Several such complexes have recently been synthesized[7-16] and most of the bonding schemes, when given, propose that electron density is transferred from the bridging carbonyl to an electron-deficient metal center,[7-10] as in **1**. The

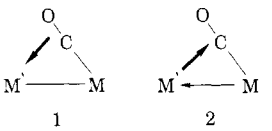

1 2

acceptor model described above for homobimetallic systems was also applied to heterobimetallic complexes and suggested that the semibridging carbonyl accepts electron density from the electron-deficient metal atom to partially alleviate the large charge imbalance that results from a dative metal–metal interaction, **2**.[2] A recent modification to the acceptor model held that the direction of electron density flow between the secondary metal center and carbonyl ligands was the same but did not rely on the existence of a metal–metal interaction.[12]

Finally, according to a recent structural analysis of semibridging carbonyl ligands, heterobimetallic complexes with coordinatively unsaturated late transition metal centers fall roughly into a category in which no significant interaction between the carbonyls and the secondary metal atom is expected.[17] The distinguishing characteristic of this type of semibridging system is that the secondary metal atom is not expected to donate electrons efficiently to the CO π^* orbitals. Coordinatively unsaturated metal centers, which are electron deficient by EAN standards, and late transition metals, which possess contracted metal orbitals, fit this description. Clearly, further study of the electronic structure of such heterobimetallic carbonyl complexes is warranted.

The electronic structures of the following four complexes are reported: (tmed)$CuCo(CO)_4$ (**3**: tmed = *N,N,N',N'*-tetramethylethylenediamine),[7] $(PPh_3)_2CuMo(CO)_3(\eta^5\text{-}C_5H_5)$[8] (**4**), $(PPh_3)_2MoRh(CO)_3(\eta^5\text{-}C_5H_5)$[9] (**5**), and (tmed)$CuMo(CO)_3(\eta^5\text{-}C_5H_5)$[10] (**6**) (the phenyl groups have been omitted from the drawings of **4** and **5** for clarity). In addition to the question of

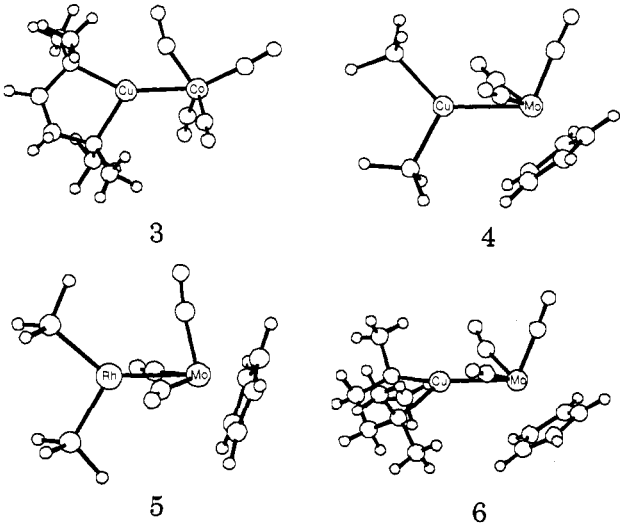

3 4 5 6

the electronic interaction between the carbonyl and secondary metal center, we chose to address several additional issues including whether the short metal–metal distances observed in some of these complexes reflect multiple bond character, strong CO bridging interactions, or both. Also of interest is why the Cu(I) center in **3** adopts a nearly square planar coordination geometry rather than the more common tetrahedral geometry.

Methods

Unparametrized Fenske–Hall[18] molecular orbital (MO) calculations were performed on the Department of Chemistry's VAX 11/780 computer. All reported results are on complexes with geometries idealized to C_s symmetry, unless otherwise noted. Calculations were also performed on all complexes in the non-idealized geometries with the atomic positions taken directly from the crystal data. As expected, no significant differences were observed since the perturbations were small. To reduce the total number of functions in the calculation of **3** and **6** the tmed ligand was replaced by two NH_3 groups with N–H distances of 1.008 Å. In **4** and **5**, each phenyl group was replaced by a hydrogen atom at the standard P–H distance of 1.42 Å. The structural data for **4** were taken from the isostructural $CuW(CO)_3(PPh_3)_2(\eta^5\text{-}C_5H_5)$[8] since only the crystal structure for the latter was reported.

The basis functions for the $4d^5$ Mo(I), $4d^8$ Rh(I), and $3d^8$ Co(I) atoms were those of Richardson et al.[19] with the exponents of the valence s and p functions set to 2.20 for Mo and Rh and 2.00 for Co. The $3d^{10}$ Cu(I) functions were taken from Clementi[20] and were fit to single-ζ functions[21] with the exception of the 3d, which was fit to a double-ζ function. The 4s and 4p exponents were set at 2.00. For P, O, and C, the double-ζ

(2) Cotton, F. A. *Prog. Inorg. Chem.* **1976**, *21*, 1.
(3) (a) Klingler, R. J.; Butler, W. M.; Curtis, M. D. *J. Am. Chem. Soc.* **1978**, *100*, 5034. (b) Curtis, D. M.; Butler, W. M. *J. Organomet. Chem.* **1978**, *155*, 131. (c) Curtis, M. D.; Han, K. R.; Butler, W. M. *Inorg. Chem.* **1980**, *19*(7), 2096.
(4) Jemmis, E. D.; Pinhas, A. R.; Hoffmann, R. *J. Am. Chem. Soc.* **1980**, *102*, 2576.
(5) Part 1 of Linear Semibridging Carbonyls: Morris-Sherwood, B. J.; Powell, C. B.; Hall, M. B. *J. Am. Chem. Soc.* **1984**, *106*, 5079.
(6) Benard, M.; Dedieu, A.; Nakamura, S. *Nouv. J. Chim.* **1984**, *8*, 149.
(7) Doyle, G.; Eriksen, K. A.; VanEngen, D. *Organometallics* **1985**, *4*, 877.
(8) Carlton, L.; Lindsell, W. E.; McCullough, K. J.; Preston, P. N. *J. Chem. Soc., Chem. Commun.* **1983**, 216.
(9) Carlton, L.; Lindsell, W. E.; McCullough, K. J.; Preston, P. N. *J. Chem. Soc., Dalton Trans.* **1984**, 1693.
(10) Doyle, G.; Eriksen, K. A. *Organometallics* **1985**, *4*, 2201.
(11) Carlton, L.; Lindsell, W. E.; McCullough, K. J.; Preston, P. N. *Organometallics* **1985**, *4*, 1138.
(12) Barr, R. D.; Marder, T. B.; Orpen, A. G.; Williams, I. D. *J. Chem. Soc., Chem. Commun.* **1984**, 112.
(13) Aldridge, M. L.; Green, M.; Howard, J. A.; Pain, G. N.; Porter, S. J.; Stone, F. G. A.; Woodward, P. *J. Chem. Soc., Dalton Trans.* **1982**, 1333. Madach, T.; Fischer, K.; Vahrenkamp, H. *Chem. Ber.* **1980**, *113*, 3235.
(14) Roberts, D. A.; Mercer, W. C.; Zahurak, S. M.; Geoffroy, G. L.; DeBrosse, C. W.; Cass, M. E.; Pierpont, C. G. *J. Am. Chem. Soc.* **1982**, *104*, 910.
(15) Werner, H.; Roll, J.; Linse, K.; Ziegler, M. L. *Angew. Chem., Int. Ed. Engl.* **1983**, *22*, 982.
(16) Doyle, G.; Eriksen, K. A.; Modrick, M.; Ansell, G. *Organometallics* **1982**, *1*, 1613.
(17) Crabtree, R. H.; Lavin, M. *Inorg. Chem.* **1986**, *25*, 805. The specific category referred to is Crabtree's type III linear semibridging carbonyls.
(18) Hall, M. B.; Fenske, R. F. *Inorg. Chem.* **1972**, *11*, 768.
(19) Richardson, J. W.; Nieuwpoort, W. C.; Powell, W. W.; Edgell, W. F. *J. Chem. Phys.* **1962**, *36*, 1057. Richardson, J. W.; Blackman, M. J.; Ranochak, J. E. *J. Chem. Phys.* **1973**, *58*, 3010 and supplement.
(20) Clementi, E. J. *IBM J. Res. Dev.* **1965**, *9*, 2 and supplement.
(21) Fenske, R. F.; Radtke, D. D. *Inorg. Chem.* **1968**, *7*, 479.

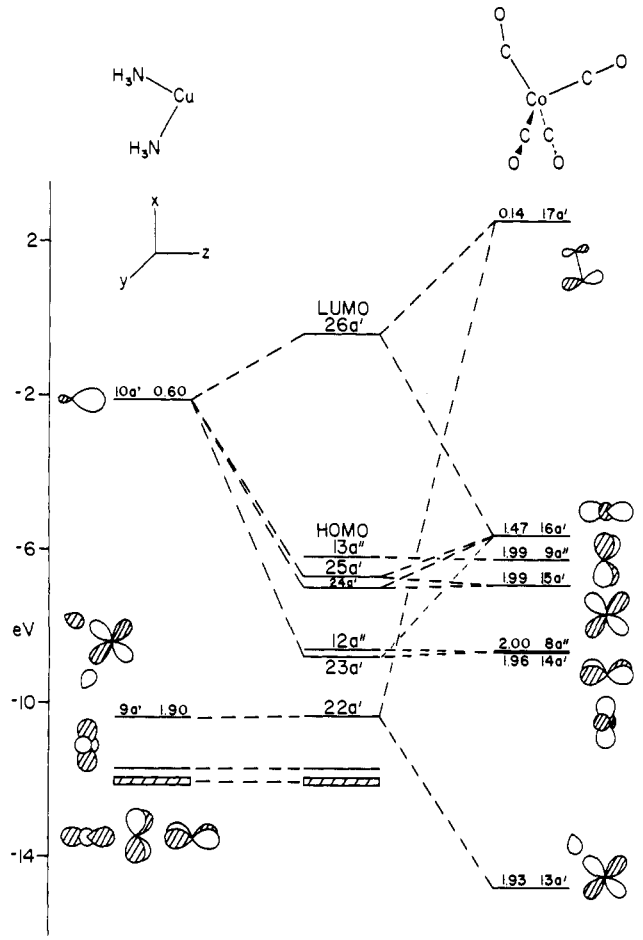

Figure 1. Molecular orbital diagram of $(NH_3)_2CuCo(CO)_4$ showing the interaction between $(NH_3)_2Cu^+$ and $Co(CO)_4^-$. The carbonyl π^* orbitals of the "t_2" set are omitted from the drawings to avoid clutter. Significant Mulliken gross populations are listed with the fragment orbitals.

functions of Clementi[22] were also fit to single-ζ functions except for the valence p, which remained as double-ζ functions. The orbital exponent for H was 1.20. Mulliken population analysis[23] was used in the calculations to determine gross and overlap populations in addition to individual atomic charges.

Results and Discussion

(tmed)CuCo(CO)$_4$. Figure 1 shows the results of a Fenske–Hall MO calculation on our model of **3** in which the results in the atomic basis have been transformed into the molecular basis for the two fragments seen on the sides of the diagram. The cobalt fragment, **8**, is represented as an anionic d^{10} species, $Co(CO)_4^-$. The "e" (14a', 8a") and "t_2" (15a', 9a", 16a') orbitals of the roughly tetrahedral fragment are doubly occupied prior to interaction, and 17a', the bent carbonyl ligand's π^* orbital in the xz plane, is the LUMO. The copper fragment, **7**, is also a d^{10} species, $(tmed)Cu^+$. The 9a', a metal–ligand antibonding orbital, is the HOMO and 10a', a metal sp_z hybrid, is the LUMO.

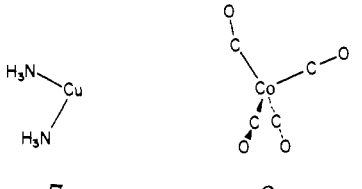

7 8

An important interaction between the two fragments is the antibonding Cu–Co d_{xz} interaction in 22a'. This Cu–Co antibonding MO is stabilized by one of the CO ligands which has moved out over the metal–metal bond and offered one lobe of its π^* orbital to the Cu d_{xz} orbital. In the process, a substantial amount of electron density (0.14 e$^-$) is transferred primarily from the Cu d_{xz} orbital (9a' of **7**) to the CO π^* orbital (17a' of **8**), as indicated by the Mulliken gross populations of the fragment MOs. The contour plot of 22a' in Figure 2 illustrates the overlap of these two interacting orbitals.[24]

The most important Cu–Co interactions are distributed among three MOs: 25a', 24a', and to a lesser extent 23a'. The gross populations indicate that a large amount of electron density (0.6 e$^-$) is transferred from **8**, primarily through the Co d_{z^2} orbital, to the LUMO of **7**. Figure 2 shows linear combinations of MOs 25a' and 24a' taken to separate out the bonding and nonbonding contributions of **8** with 10a' of **7**.[26] The former shows that the Co π^* component of the "t_2" orbital participates in the interaction with the Cu sp_z orbital. The MO analysis did not contain a significant metal–metal interaction of π symmetry, indicating that the short Cu–Co bond length is due entirely to the strongly bridging carbonyl ligand.

The bonding description of **3**, represented in Figure 1, resembles the acceptor model, **2**, described above. The cobalt fragment acts as the donor in a dative metal–metal interaction. A CO ligand then bridges the metal–metal bond to accept electron density from the secondary metal center into one of its empty π^* orbitals.

It is important to realize that the MO energies and the Mulliken gross populations listed above the fragment MO levels in Figure 1 do not depend on the partitioning of electrons between the fragments. Whether one chooses to describe the interaction of the fragments as one of ionic $Cu(NH_3)_2^+$ and $Co(CO)_4^-$ fragments or of neutral radical $Cu(NH_3)_2^\bullet$ and $Co(CO)_4^\bullet$ fragments does not affect the values obtained from the Mulliken population analysis or the solution of the secular equation. What does change is the amount of electron density lost or gained by fragment orbitals with respect to the starting (isolated) fragment orbitals. For example, the 10a' orbital of the copper fragment, **7**, in Figure 1 is unoccupied prior to interaction with the cobalt fragment, **8**, when the fragment is designated as an ionic $Cu(NH_3)_2^+$ species. Upon interaction, 10a' gains 0.60 electron from the cobalt fragment. If, instead, we choose to classify the interaction as one between neutral radical species, the 10a' orbital of **7** is singly occupied prior to interaction with **8**. Upon interaction, the Mulliken gross populations of orbital 10a' will still be 0.60 electron, but will instead reflect that the radical copper fragment has *lost* 0.40 electron. In terms of the qualitative description of the interaction we say that for the case of the ionic fragments the interaction is dative with the cobalt fragment donating electrons to the copper fragment. For the neutral fragments, the interaction is more covalent in nature and is polarized toward the more electronegative cobalt fragment.[27] Regardless of how the electrons are partitioned in the fragment calculations, the Mulliken gross populations of the fragment orbitals remain unchanged. In this paper we will use closed shell fragments that most resemble the final charge distribution.

To determine why the planar coordination geometry around the Cu atom was preferred over the more common tetrahedral geometry, calculations were carried out on the complex in the latter

(22) Clementi, E. J. *J. Chem. Phys.* **1964**, *40*, 1944.
(23) Mulliken, R. S. *J. Chem. Phys.* **1955**, *23*, 1833, 1841.
(24) All contour plots were generated with the program MOPLOT. Lichtenberger, D. L. Ph.D. Dissertation, University of Wisconsin, Madison, WI, 1974. The program is available from the Quantum Chemistry Program Exchange, Indiana University, Bloomington, IN 47401, Program 284.
(25) Wells, A. F. *Structural Inorganic Chemistry*, 5th ed.; Oxford University Press: Oxford, England, 1984; p 1289.
(26) The single-determinant Hartree–Fock wave function is invariant to unitary transformations of the MOs. Taking the linear combination of two MOs is equivalent to operating on the set of MOs with a unitary matrix **U** which is a block diagonal unit matrix containing a unitary 2 × 2 block of normalized weighting coefficients. See: Szabo, A.; Ostlund, N. S. *Modern Quantum Chemistry: Introduction to Advanced Electronic Structure Theory*; Macmillan Publishing Co.: New York, 1982; p 120.
(27) The interaction of hydrogen and fluorine can be viewed the same way. As ions, the nature of the interaction is dative with F^- donating electrons to H^+. As neutral fragments, the interaction can be viewed as covalent with the bonding charge density strongly polarized toward the more electronegative fluorine atom.

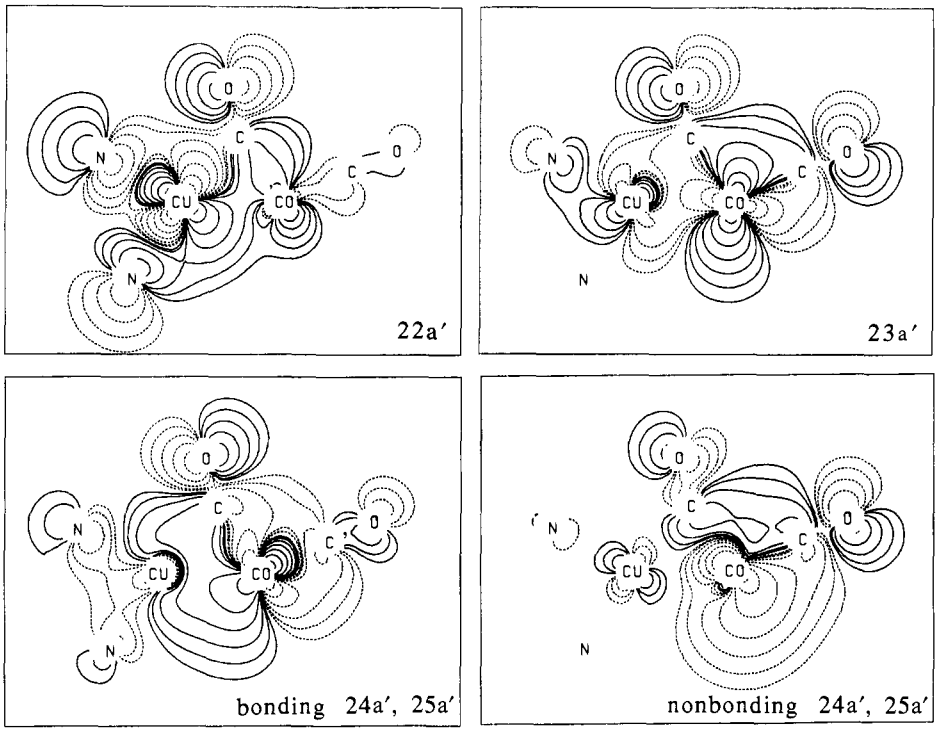

Figure 2. Contour plots for selected valence orbitals of $(NH_3)_2CuCo(CO)_4$. The lower two plots illustrate the bonding and nonbonding linear combinations of MOs 24a' and 25a'. Contours are geometric, differing by a factor of 2, with the lowest contour of 0.00781 (e Å^{-3})$^{1/2}$.

geometry. Reorientation of the copper fragment, **7**, with respect to the cobalt fragment, **8**, such that the copper atom resides in a nearly tetrahedral coordination environment involves a rotation of **7** about the Cu–Co axis by roughly 90°, followed by some minor adjustments. As a result of the reorientation, the Cu d_{yz} orbital, rather than the d_{xz} orbital, is of proper symmetry to interact with the bridging CO π^* orbital. Figure 1 shows that the d_{yz} orbital is almost 2 eV further removed from the LUMO of **8** than is the d_{xz} orbital, thereby reducing the interaction on energetic grounds. Our calculations show that if the coordination geometry around the Cu atom is tetrahedral, the amount of electron density transferred into 17a' of **8** is also reduced by about one-third. This reduction in the back donation affects the metal–metal density transfer as well, decreasing the density gained in 10a' by about 10%. One might therefore expect the Cu–Co distance to increase as a result of the tetrahedral coordination geometry.

The structure of **3** in solution does not exhibit the bridging interaction seen in the solid state.[7] One might, therefore, argue that packing forces play a significant role in the solid-state structure and that relief of these forces would favor a structure that is more symmetrical and does not display any bridging interaction, such as **9**. Intramolecular van der Waals energy

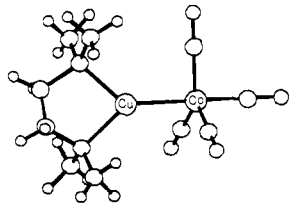

9

calculations show that the total repulsion energy of the actual bridging structure is approximately 70 kcal/mol higher than that in **9** and that 90% of this repulsion energy is due to the Cu–bridging carbonyl C contact. Inspection of the packing fails to reveal any intermolecular cause for the bridging interaction. Rather, the bridging structure is the result of more favorable electronic interactions.

The structure in solution is probably the result of the coordination of a polar solvent molecule (even a weakly polar solvent such as CH_2Cl_2) to the unsaturated copper fragment. The solvent molecule fills up the vacant coordination site and contributes to the steric bulk of the copper fragment, thereby preventing a

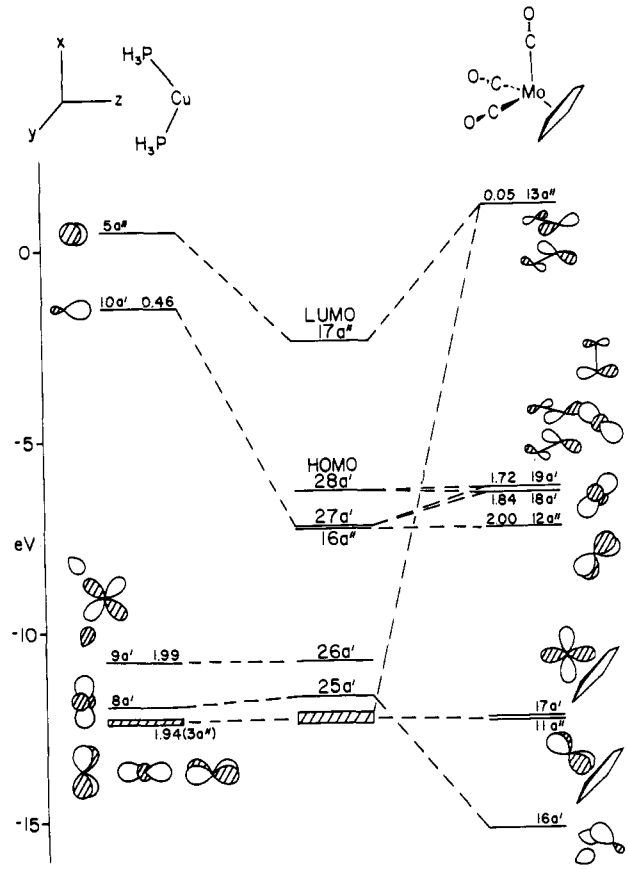

Figure 3. Molecular orbital diagram of $(PH_3)_2CuMo(CO)_3(\eta^5\text{-}C_5H_5)$ constructed from the $(PH_3)_2Cu^+$ and $Mo(CO)_3(\eta^5\text{-}C_5H_5)^-$ fragments. The Mo z axis is oriented along the pseudo-C_3 rotation axis of the pseudo-octahedral fragment. The carbonyl π^* orbitals of 18a' and 12a" of the t_{2g} set are not included in the fragment orbital drawings.

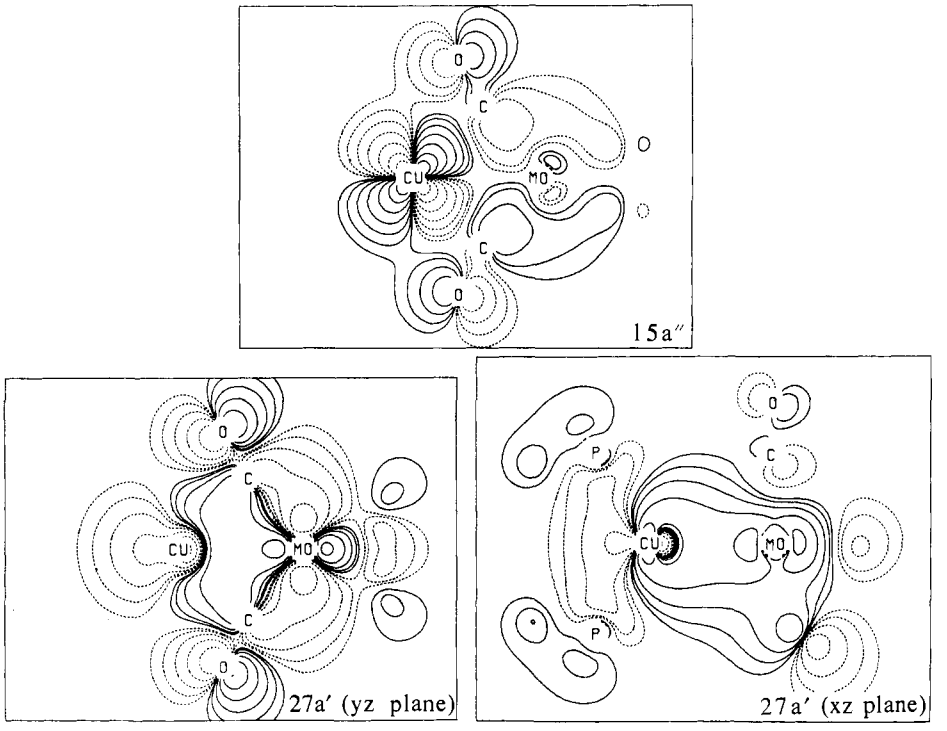

Figure 4. Contour plots for upper valence orbitals of $(PH_3)_2CuMo(CO)_3(\eta^5\text{-}C_5H_5)$. See Figure 2 for contour information.

carbonyl from the other fragment from bridging the metal–metal bond.

$(PPh_3)_2CuMo(CO)_3(\eta^5\text{-}C_5H_5)$. The structural characteristics of $(PPh_3)_2CuMo(CO)_3(\eta^5\text{-}C_5H_5)$ (**4**) are surprisingly different from those of **3**. Not only is the plane of the bridging carbonyls nearly perpendicular to the plane containing the Cu and two P atoms of **10**, but the Cu–Mo distance of 2.721 Å is roughly 0.05 Å longer than that expected for a single Cu–Mo bond. The MO diagram for $(PH_3)_2CuMo(CO)_3(\eta^5\text{-}C_5H_5)$, our model for **4**, is shown in Figure 3. The frontier orbitals of the copper fragment, **10**, are similar in character to those of **7**. In the pseudo-octahedral d^6 $Mo(CO)_3Cp^{-1}$ fragment, **11**, the 19a′ orbital is the HOMO and the 13a″ orbital is the LUMO.

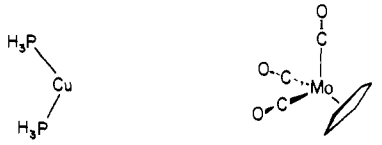

10 11

Two points about the electronic structure of **4** are are immediately obvious from Figure 3. First, the dative Mo–Cu interaction does not involve the transfer of as much electron density as was seen in **3**. Despite the fact that the "t_{2g}" (12a″, 18a′, 19a′) orbitals contain a higher percentage of d character than the corresponding "t_2" set of **8**, the larger energy difference (by about 1 eV) between these orbitals and 10a′ of the copper fragment dominates the interaction term, and as a result less electron density is transferred. Second, the back donation of density from the Cu to the bridging carbonyls is very small. The Cu orbital that participates in this interaction is not the L–M antibonding 9a′ orbital as it was in **3** but rather the nonbonding 3a″, which is lower in energy. Despite this energy difference, the 3a″–13a″ gap is similar to the 9a′–17a′ gap in **3**, and the lack of interaction is instead due to the decreased orbital overlap (0.081 in **4**, 0.117 in **3**) that is a consequence of the increased Cu–C distance (2.3 Å in **4**, 2.0 Å in **3**).

The contour plot of 15a″ in Figure 4 illustrates the lack of positive overlap between the "bridging" carbonyl π^* orbitals and the Cu d_{yz} orbital. Even though these two carbonyl ligands lie below the *yz* plane containing the two metal atoms and the contour plot is taken in this plane, a separate contour plot taken in the plane containing the Cu and two bridging carbonyl carbon atoms revealed no significant difference between the two. The plots of 27a′ in the two perpendicular planes show that two of the three carbonyls participate in the metal–metal bond through their contribution to the "t_{2g}" orbitals.

While the bulky PPh_3 groups prevent **10** from interacting with **11** in the same plane as the bridging COs, one might wonder if the long metal–metal distance is also a reflection of their steric influence. We have already indicated that the difference in energy between the interacting orbitals plays an important role, but do the PPh_3 ligands also restrict the overlap of the Cu–Mo orbitals? The off-diagonal Fock matrix terms suggest that they do not since the sum of $\langle 10a'|H|19a'\rangle^2$ and $\langle 10a'|H|18a'\rangle^2$ from **4** is larger than the corresponding sum of $\langle 10a'|H|16a'\rangle^2$ and $\langle 10a'|H|15a'\rangle^2$ from **3**. In this case, the energy difference between interacting orbitals, manifest in the denominator of the interaction term, controls the degree of interaction.[28] Since the molybdenum fragment, **11**, of **4** uses the stabilized "t_{2g}" set to interact with the Cu fragment while the cobalt fragment, **8**, of **3** uses the destabilized "t_2" set, the latter interaction term is larger. In addition, the metal–metal distance in **5**, the Rh–Mo analogue of **4**, at 2.558 Å, is more than 0.1 Å shorter than what is expected for a single Rh–Mo bond based on the average of the Mo–Mo and Rh–Rh bond lengths observed in metals.[25] Clearly, the steric influence of the PPh_3 groups on the metal–metal interaction is minimal in this geometry.

$(PH_3)_2RhMo(CO)_3(\eta^5\text{-}C_5H_5)$. The short Rh–Mo bond observed in the structure of **5** prompted the authors of the original report to propose a Rh → Mo dative interaction of π symmetry in

(28) The change in the energy splitting between two atomic or fragment molecular orbitals before and after they interact is one way of measuring the extent of their interaction. Quantitatively, the energy difference is given by the second order perturbation correction to the energy,

$$\sum_{j \neq i} \frac{|H_{ij}|^2}{E_i - E_j}$$

where the numerator is the square of the Fock matrix element and the denominator is the difference in energy between the interacting fragments. See: Hoffmann, R. *Acc. Chem. Res.* **1971**, *4*, 1. While strict quantitative comparisons of matrix elements from different compounds are not appropriate, qualitative comparisons can be helpful in determining their relative influence in the interaction terms.

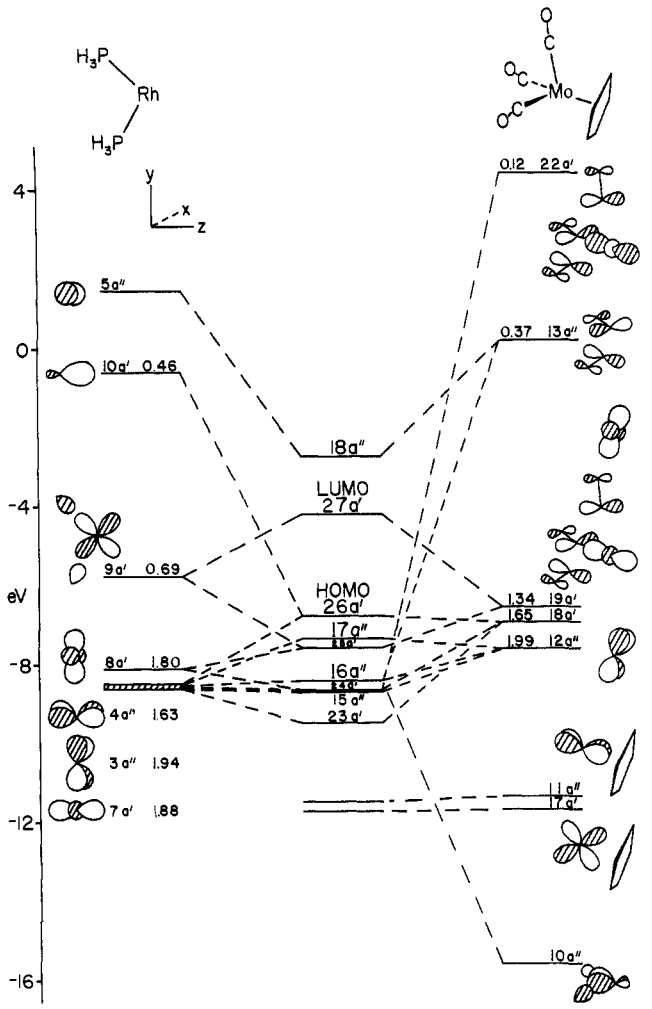

Figure 5. Molecular orbital diagram $(PH_3)_2RhMo(CO)_3(\eta^5\text{-}C_5H_5)$ constructed from $(PH_3)_2Rh^+$ and $Mo(CO)_3(\eta^5\text{-}C_5H_5)^-$. The Mo z axis is oriented along the pseudo-C_3 rotation axis of the fragment.

addition to a Rh → Mo dative interaction of σ symmetry and electron density donation from the bridging carbonyls to the Rh center. Our calculations support the presence of a dative Rh–Mo π bond but indicate that the donor/acceptor roles are reversed. The results are illustrated in Figure 5.

The replacement of the Cu atom in **10** with a Rh atom results in a fragment with two fewer electrons, which makes 8a′ the HOMO and 9a′ the LUMO. The frontier orbitals of **12** also experience a general destabilization relative to **10** which enhances the energetic compatibility of the Rh d orbitals with the Mo "t_{2g}" set and CO π^* orbitals. The dative Rh–Mo bond of σ symmetry in 26a′ involves an out-of-phase Rh d_{z^2}/Mo d_{z^2} interaction that is stabilized by the Rh sp_z orbital. The net effect is the transfer of 0.46 e^-, most of which comes from the Mo fragment, to 10a′ of the Rh fragment **12**. The contour plot of 26a′ in the yz plane

12 13

in Figure 6 illustrates both the bonding and antibonding interactions more clearly than the plot in the xz plane. Both plots fail to reveal the dative nature of the interaction since the number of contours on the Rh fragment is equal to, if not greater than, the number of contours on the Mo fragment, giving the molecular orbital the appearance of a covalent interaction. The number of contours on the Rh fragment is larger than one might expect in

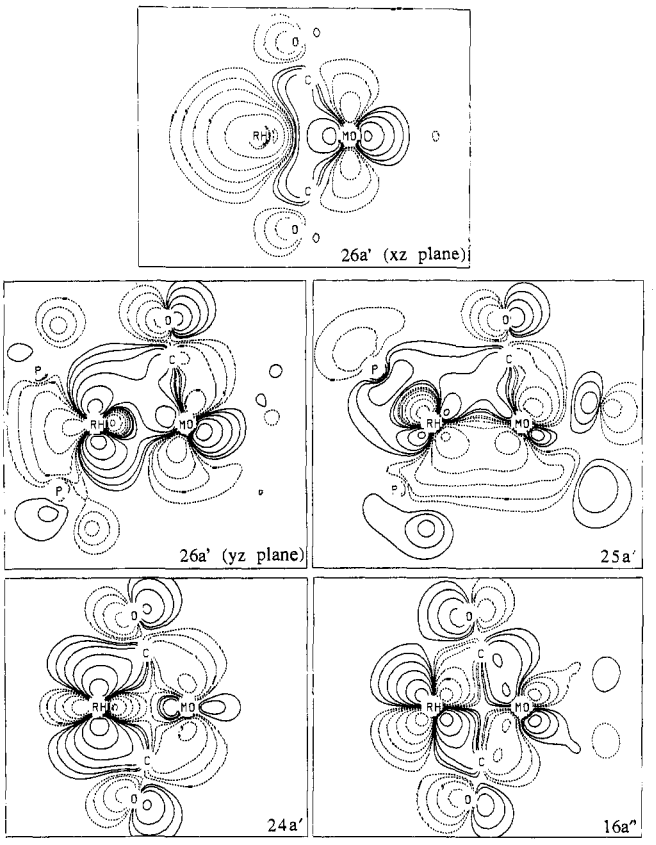

Figure 6. Contour plots for upper valence MOs of $(PH_3)_2RhMo(CO)_3(\eta^5\text{-}C_5H_5)$. See Figure 2 for contour information.

this case because of the participation of 7a′, the occupied Rh d_{z^2} orbital, in 26a′.

The subtle details of the dative Rh–Mo interaction of π symmetry in 25a′ are not obvious in the simplified MO diagram of Figure 5. The primary interaction is between 9a′ of the Rh fragment, **12**, and 19a′ of the Mo fragment, **13**. The molybdenum fragment, **13**, obtains its π symmetry (with respect to the metal–metal interaction) from a small combination of the d_{z^2} character present in 19a′ plus a small contribution from the d_{yz} orbital in 17a′. As the contour plot illustrates, even the terminal CO π^* orbital participates in the metal–metal interaction to a small degree. The amount of electron density transferred to the 9a′ orbital is large and comes primarily from 19a′ of **13**. Additional contours are added to the Rh fragment from the contribution of 8a′ to the MO, which also makes this interaction look more covalent than dative.

Figure 5 illustrates that the large metal–metal interaction is accompanied by substantial back donation of electron density to the bridging carbonyls. The 16a″ MO consists of an antibonding interaction between 4a″ of **12** and 10a″ of **13**. The MO is also stabilized to a small extent by 12a″ of **13** and to a large extent by 13a″ (also of **13**), the latter being the largest percent character contributor of any fragment orbital of **13** to the MO. Nearly 0.4 e^- moves from 4a″ of **12** to 13a″ of **13**.

Additional back donation to one of the "t_{2g}*" set, 22a′, is possible due to the relatively high energy of the Rh fragment orbitals. The interaction appears in MO 24a′ and, like 16a″, involves the participation of several fragment orbitals. The major participant from the Rh fragment, **12**, is 8a′, from which most of the electron density that ends up in 22a′ comes. The 7a′ contributes only one-fifth of the percent character of 8a′ but provides the remainder of the donated density. The major participant from the Mo fragment, **13**, is the "t_{2g}" counterpart of 22a′, 18a′, as the contour plot in Figure 6 reflects.

The structure of the paramagnetic nickel analogue, $MNi(CO)_3(PPh_3)_2(\eta^5\text{-}C_5H_5)$ (M = W, Mo), was recently reported along with an extended Hückel MO study on the tungsten com-

plex.[11] Although the authors acknowledged the existence of a short metal-metal bond distance, their EHMO study failed to account for its presence. Their study concluded that the metal fragments were held together by a combination of relatively weak Ni-W and C-Ni interactions. Our calculations show that while this is true for the Cu-Mo analogue, **4**, the Ni complex contains the strong interactions characteristic of the Rh complex, **5**. The MO diagram from the EH study illustrated that the Ni fragment orbitals were sufficiently destabilized to allow the interaction of the Ni 3d orbitals with the "t_{2g}" set of the tungsten fragment (similar to the Rh 4d/Mo "t_{2g}" set interaction seen in Figure 5 although to a more limited extent). The key interaction that is present in both complexes is the metal-metal interaction of π symmetry. The additional electron present in the Ni complex singly occupies the metal-metal π antibonding orbital 27a′ which therefore only partially cancels the corresponding bonding interaction. Taken together with the interaction of σ symmetry (an interaction not shown in the EHMO diagram) the total direct metal-metal interaction possesses a bond order of roughly 1.5, which is clearly a significant interaction. Strong back donation of electron density to the bridging carbonyls further contributes to the short metal-metal bond distance that is observed in the complex.

(tmed)CuMo(CO)$_3$(η^5-C$_5$H$_5$). On the basis of the bonding descriptions presented so far, we might now ask what would be expected from the interaction of a Mo(CO)$_3$(η^5-C$_5$H$_5$)$^-$ fragment with Cu(tmed)$^+$, a fragment less sterically bulky than M(PPh$_3$)$_2^+$. The most obvious expectation might be that the Cu, N, N plane would approach the Mo fragment in the plane of two carbonyl ligands, **14**, to take advantage of the destabilized Cu-N antibonding HOMO and interact with the virtual carbonyl π^* orbitals.

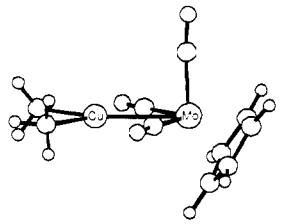

14

The crystal structure reported by Doyle and Eriksen,[10] **6**, shows instead that the Cu fragment approaches Mo from below the plane containing the two carbonyls such that the final geometry of the Mo fragment resembles the four-legged piano stool. The Cu-Mo bond distance of 2.59 Å is substantially shorter than that found in (PPh$_3$)$_2$CuMo(CO)$_3$(η^5-C$_5$H$_5$), **4**. Our calculations suggest that if steric effects are not taken into account, the most favorable geometry is the coplanar orientation, **14**. In this geometry the overlap of the Cu-L antibonding orbital with the bridging CO π^* orbitals is much larger than that in the four-legged piano stool geometry (0.121 vs 0.086) allowing twice as much electron density to be transferred from the copper fragment to the carbonyls. The steric effects of the tmed group, however, are significant and the complex is forced to swing the tmed group down below the plane of the bridging carbonyls. The back donation to the carbonyls in **6** is too small (it is similar in magnitude to that seen in **4**) to be a significant factor in the short Cu-Mo bond distance. The short Cu-Mo bond distance is instead the result of the lower energy Cu sp$_z$ hybrid interacting with the Mo t_{2g} set. The change from phosphines to amines coordinated to Cu changes the relative amount of Cu 4s and 4p character in the hybrid from one-third 4s and two-thirds 4p to two-thirds 4s and one-third 4p, respectively. The greater 4s character in the amine-coordinated Cu sp$_z$ hybrid is responsible for the lower energy of this orbital, the greater interaction with the Mo t_{2g} set, and hence the short metal-metal bond.

Conclusion

We have shown that heterobimetallic carbonyl complexes with coordinatively unsaturated late transition metal centers—centers not normally thought of as good electron density donors—are capable of donating electron density back to the virtual carbonyl π^* orbitals of an adjacent metal center. For the molecules studied in this work, the back donation was accompanied by a dative metal-metal interaction involving the transfer of electron density from the coordinatively saturated fragment to the LUMO of unsaturated fragment.

Acknowledgment. The authors thank the Robert A. Welch Foundation (Grant No. A-648) and the National Science Foundation (Grant No. CHE 86-19420) for their support.

The Silanoic Acid Dimer (HSiOOH)$_2$: A Simple Molecular System Incorporating Two Very Strong Hydrogen Bonds

Edward T. Seidl† and Henry F. Schaefer III*

Contribution CCQC No. 29 from the Center for Computational Quantum Chemistry, School of Chemical Sciences, University of Georgia, Athens, Georgia 30602. *Received June 21, 1988*

Abstract: Ab initio molecular electronic structure theory has been used to predict and characterize the remarkable species (HSiOOH)$_2$. The dissociation energy to two silanoic acid monomers is predicted to be D_0 = 25 kcal/mol, twice that observed for the well-characterized valence isoelectronic formic acid dimer. Fundamental vibrational frequencies allowed in the infrared spectrum are predicted as follows: ν(O-H) = 2905 cm^{-1}, ν(Si=O) = 1229 cm^{-1}, and ν(Si-O) = 955 cm^{-1}. By avoiding formal double bonds to silicon, a much lower energy cyclic isomer of the silanoic acid dimer may be found, and this structure is also theoretically characterized.

An important new direction in chemistry for the past decade or more has been the exploration of molecules in which one or more carbon atoms from a hydrocarbon compound has been replaced by silicon. One such obvious example is silanoic acid, HSiOOH, the silicon analogue of formic acid, HCOOH. The silanoic acid molecule was first observed in the laboratory by Withnall and Andrews,[1,2] using the technique of matrix isolation infrared spectroscopy. The observations of Withnall and Andrews were bolstered by the ab initio quantum mechanical predictions

† Robert S. Mulliken Graduate Fellow.

(1) Withnall, R.; Andrews, L. *J. Phys. Chem.* **1985**, *89*, 3261.
(2) Withnall, R.; Andrews, L. *J. Am. Chem. Soc.* **1985**, *107*, 2567.

0002-7863/89/1511-1569$01.50/0